8-methoxy-1,2,3,4-etrahydroquinoline, based on ^{13}C–nuclear magnetic resonance analysis of the crude reaction product (figs. S5 and S6). Secondary alcohols likewise participated readily in the Mitsunobu and aza-annulation reactions, **9e→10e→11e** (entry 5). This two-step sequence, when conducted using the chiral alcohol **9f**, showed no loss of stereochemical integrity (entry 6). Incorporation of a heteroatom into the ring closure, e.g., **9g→10g→11g** (entry 7), did not perturb the chemistry and provided easy access to the dihydrobenzoxazine class of heterocycles. The yield declined somewhat for making the five-membered dihydroindole **11h** from alcohol **9h** (entry 8), but improved for the seven-membered tetrahydrobenzazepine **11i** from **9i** (entry 9).

As a beginning toward gaining insight into the mechanism of the amination, a 1:1 mixture of naphthalene (**7q**) and **7q**-d_8 was treated with a limited amount of amination reagent (**4a**, 0.5 equiv.) under otherwise standard reaction conditions. Samples were taken and quenched at 10, 20, 30, and 40 min. Analysis via selected ion monitoring–liquid chromatography–mass spectrometry revealed that the product ratios remained constant at ~1:1, a ratio inconsistent with an organometallic C-H activation pathway, which would typically manifest ~3:1 or higher ratios (*40*, *41*). Based on DFT calculations, we previously suggested that aziridination of alkenes involves the dirhodium-nitrenoid intermediate **B** shown in Fig. 4 that arises from overall NH transfer from the DPH-aminating reagent to the dirhodium catalyst (*33*). In contrast, reaction of *O*-tosylhydroxylamine reagents with the dirhodium catalyst favor intermediate **A** because TsO^- is weakly basic and the equilibrium with intermediate **B** lies far to the left. The chemoselectivity might be explained by the more electrophilic nature of intermediate **A** versus nitrenoid **B**. This preliminary hypothesis is consistent with the observation that moderate-to-strong bases such as K_2CO_3, Et_3N, and pyridine completely inhibit amination, but not aziridination. Moreover, addition of TsOH (1.5 equiv.) to the reaction of **1** with 2,4-DNPONHMe (**12**) produced only the arene amination adduct **5** and no aziridine. As an additional control, it was shown that the presence of 2,4-DNP-OH (1.5 equiv.) did not alter the reaction manifold in favor of aziridination when **4a** was used as the aminating reagent and only **5** was observed.

It was also instructive to compare our methodology with the intermolecular Rh-catalyzed amination procedure of Du Bois to gain a perspective on their respective complementary chemoselectivities (Fig. 4) (*42*). Both have similar efficiency using *p*-ethylanisole (**13**), but the Du Bois procedure leads to benzylic C-H insertion only, whereas our methodology gives arene amination exclusively, providing **15** and **16** in a combined 67% yield.

The influence of ligands and counterions on the reactivity of organometallics is well precedented (*43*, *44*). However, examples of such dramatic bifurcation of the reaction manifold are rare and warrant closer study to understand the energetics and full synthetic potential of this metalloid-nitrogen umpolung for direct arene aminations.

REFERENCES AND NOTES

1. R. Hili, A. K. Yudin, *Nat. Chem. Biol.* **2**, 284–287 (2006).
2. A. Ricci, Ed., *Amino Group Chemistry: From Synthesis to the Life Sciences* (Wiley-VCH, 2008).
3. R. J. Angelici, *Reagents for Transition Metal Complex and Organometallic Synthesis* (Wiley-Interscience, New York, 1990), vol. 28.
4. A. Dalla Cort *et al.*, *J. Org. Chem.* **70**, 8877–8883 (2005).
5. N. R. Candeias, L. C. Branco, P. M. P. Gois, C. A. M. Afonso, A. F. Trindade, *Chem. Rev.* **109**, 2703–2802 (2009).
6. J. F. Hartwig, S. Shekhar, Q. Shen, F. Barrios-Landeros, *Chem. Anilines* **1**, 455–536 (2007).
7. Y.-S. Xie *et al.*, *Tetrahedron Lett.* **54**, 5151–5154 (2013).
8. J. Yu, P. Zhang, J. Wu, Z. Shang, *Tetrahedron Lett.* **54**, 3167–3170 (2013).
9. T. Daskapan, *ARKIVOC* **2011**, 230–262 (2011).
10. K. Kunz, U. Scholz, D. Ganzer, *Synlett* (15): 2428–2439 (2003).
11. J. F. Hartwig, *Acc. Chem. Res.* **41**, 1534–1544 (2008).
12. D. S. Surry, S. L. Buchwald, *Angew. Chem. Int. Ed.* **47**, 6338–6361 (2008).
13. N. Xia, M. Taillefer, *Angew. Chem. Int. Ed.* **48**, 337–339 (2009).
14. X. Zeng, W. Huang, Y. Qiu, S. Jiang, *Org. Biomol. Chem.* **9**, 8224–8227 (2011).
15. R. J. Lundgren, M. Stradiotto, *Aldrichim Acta* **45**, 59–65 (2012).
16. T. Maejima *et al.*, *Tetrahedron* **68**, 1712–1722 (2012).
17. H. M. L. Davies, X. Dai, Synthetic reactions via C-H bond activation: Carbene and nitrene C-H insertion, in *Comprehensive Organometallic Chemistry III*, R. H. Crabtree, D. M. P. Mingos, Eds. (Elsevier, 2007), vol. 10, pp. 167–212.
18. J. Jiao, K. Murakami, K. Itami, *ACS Catal.* **6**, 610–633 (2016).
19. P. Starkov, T. F. Jamison, I. Marek, *Chemistry* **21**, 5278–5300 (2015).
20. W. C. P. Tsang, N. Zheng, S. L. Buchwald, *J. Am. Chem. Soc.* **127**, 14560–14561 (2005).
21. K. Inamoto, T. Saito, M. Katsuno, T. Sakamoto, K. Hiroya, *Org. Lett.* **9**, 2931–2934 (2007).
22. G. Brasche, S. L. Buchwald, *Angew. Chem. Int. Ed.* **47**, 1932–1934 (2008).
23. K. Inamoto, T. Saito, K. Hiroya, T. Doi, *J. Org. Chem.* **75**, 3900–3903 (2010).
24. R. Shrestha, P. Mukherjee, Y. Tan, Z. C. Litman, J. F. Hartwig, *J. Am. Chem. Soc.* **135**, 8480–8483 (2013).
25. Y. Xue *et al.*, *Eur. J. Org. Chem.* **2014**, 7481–7488 (2014).
26. Z. Chen *et al.*, *Org. Chem. Front.* **2**, 1107–1295 (2015).
27. Y. Park, K. T. Park, J. G. Kim, S. Chang, *J. Am. Chem. Soc.* **137**, 4534–4542 (2015).
28. K. Shin, H. Kim, S. Chang, *Acc. Chem. Res.* **48**, 1040–1052 (2015).
29. F. Sun, Z. Gu, *Org. Lett.* **17**, 2222–2225 (2015).
30. C. Suzuki, K. Hirano, T. Satoh, M. Miura, *Org. Lett.* **17**, 1597–1600 (2015).
31. K. Takamatsu, K. Hirano, T. Satoh, M. Miura, *J. Org. Chem.* **80**, 3242–3249 (2015).
32. N. A. Romero, K. A. Margrey, N. E. Tay, D. A. Nicewicz, *Science* **349**, 1326–1330 (2015).
33. J. L. Jat *et al.*, *Science* **343**, 61–65 (2014).
34. Z. Yang, *Synlett* **25**, 1186–1187 (2014).
35. O. R. S. John *et al.*, *Org. Lett.* **9**, 4009–4012 (2007).
36. J. Mendiola *et al.*, *Org. Process Res. Dev.* **13**, 263–267 (2009).
37. L. A. Carpino, *J. Am. Chem. Soc.* **82**, 3133–3135 (1960).
38. M. Cherest, X. Lusinchi, *Tetrahedron Lett.* **30**, 715–718 (1989).
39. M. Kawase, Y. Kikugawa, *Chem. Pharm. Bull. (Tokyo)* **29**, 1615–1623 (1981).
40. W. D. Jones, *Acc. Chem. Res.* **36**, 140–146 (2003).
41. E. M. Simmons, J. F. Hartwig, *Angew. Chem. Int. Ed.* **51**, 3066–3072 (2012).
42. C. G. Espino, K. W. Fiori, M. Kim, J. Du Bois, *J. Am. Chem. Soc.* **126**, 15378–15379 (2004).
43. L. S. Hegedus, *Transition Metals in the Synthesis of Complex Organic Molecules* (University Science Books, 1994), pp. 16–22.
44. C. G. Espino, J. Du Bois, *Angew. Chem. Int. Ed.* **40**, 598–600 (2001).

ACKNOWLEDGMENTS

J.R.F. thanks NIH (grant HL034300, HL111392, DK038226) and the Robert A. Welch Foundation (grant I-0011) for funding. L.K. gratefully acknowledges the generous financial support of Rice University, NIH (grant R01 GM-114609-01), NSF (CAREER:SusChEM CHE-1455335), the Robert A. Welch Foundation (grant C-1764), American Chemical Society Petroleum Research Fund (grant 51707-DNI1), Amgen (2014 Young Investigators' Award to L.K.), and Biotage (2015 Young Principal Investigator Award). A provisional patent application (patent no. 62/360,859) has been submitted and assigned jointly to University of Texas Southwestern and Rice University.

SUPPLEMENTARY MATERIALS

www.sciencemag.org/content/353/6304/1144/suppl/DC1
Materials and Methods
Figs. S1 to S4
Table S1
References (*45*–*61*)

12 April 2016; accepted 18 August 2016
10.1126/science.aaf8713

ANTIBIOTIC RESISTANCE

Spatiotemporal microbial evolution on antibiotic landscapes

Michael Baym,[1] Tami D. Lieberman,[1]* Eric D. Kelsic,[1] Remy Chait,[1]† Rotem Gross,[2] Idan Yelin,[2] Roy Kishony[1,2,3]‡

A key aspect of bacterial survival is the ability to evolve while migrating across spatially varying environmental challenges. Laboratory experiments, however, often study evolution in well-mixed systems. Here, we introduce an experimental device, the microbial evolution and growth arena (MEGA)–plate, in which bacteria spread and evolved on a large antibiotic landscape (120 × 60 centimeters) that allowed visual observation of mutation and selection in a migrating bacterial front. While resistance increased consistently, multiple coexisting lineages diversified both phenotypically and genotypically. Analyzing mutants at and behind the propagating front, we found that evolution is not always led by the most resistant mutants; highly resistant mutants may be trapped behind more sensitive lineages. The MEGA-plate provides a versatile platform for studying microbial adaption and directly visualizing evolutionary dynamics.

The worldwide increase in antibiotic resistance has motivated numerous studies aimed at understanding the phenotypic and genotypic evolution of antibiotic resistance (*1*–*7*). These experiments have shed light on the trade-offs constraining adaptive evolution in single- and multidrug environments (*5*, *6*, *8*, *9*). However, most of our current knowledge about the evolution of resistance is based on laboratory setups with well-mixed environments (*1*–*7*, *10*, *11*).

In natural and clinical settings, bacteria migrate between spatially distinct regions of selection

(*5*, *6*, *8*, *9*, *12*, *13*). Theoretical models show that spatially structured pressures change the nature of selection: Instead of competing with its neighbors for limited resources, an adapted individual needs only to be the first with the capability to venture and survive in a new region (*14*, *15*). A pioneering study focusing on small population sizes showed that structured microenvironments increase the rate of adaptation to antibiotics through highly reproducible genetic changes (*9*). It is unknown how evolution is shaped by the diversification potential and differences in adaptive constraints of large populations in spatial environments.

Here, we present a device for the evolution of bacteria that allows migration and adaptation in a large, spatially structured environment. The microbial evolution and growth arena (MEGA)–plate consists of a rectangular acrylic dish, 120 × 60 cm, in which successive regions of black-colored agar containing different concentrations of antibiotics are overlaid by soft agar allowing bacterial motility (Fig. 1A). Motile bacteria inoculated at one location on the plate deplete nutrients locally and then spread by chemotaxis to other regions (*16*). Only increasingly resistant mutants can spread into sections containing higher levels of antibiotic. The large size of the plate serves two purposes: It provides for a large population and mutational supply, and it maintains the antibiotic gradient despite diffusion (drug diffusion time scales quadratically with distance while the bacterial front advances linearly; thus, the large plate size prevents the antibiotic gradient from equilibrating over the duration of the experiment). Once a mutant has exhausted the resources of a region of the plate, other mutants do not meaningfully migrate by chemotaxis to that region (because they move diffusively without a nutrient gradient). In this manner, mutational lineages can block each other physically—a phenomenon notably observed in biofilm formation (*17*). This partitioning of mutants into stable spatial domains also enables sampling of individual mutants for later analysis. Using periodic photography of the plate, we constructed time-lapse movies of evolution (movie S1). Combining these with analysis of isolates, this system allows reconstruction of the phenotypic and genotypic evolutionary histories of evolving bacteria.

Challenging bacteria in spatial gradients of antibiotics leads to large increases in resistance through sequential adaptive steps across competing lineages (Fig. 1 and movie S1). We first set up the MEGA-plate with symmetric four-step gradients of trimethoprim (TMP) or ciprofloxacin (CPR) proceeding inward with order-of-magnitude increases in concentration per step [Fig. 1A; TMP: 0, 3, 30, 300, and 3000 × wild-type minimum inhibitory concentration (MIC); CPR: 0, 20, 200, 2000, and 20,000 × MIC] and inoculated the drug-free regions with *Escherichia coli*. Bacteria swim and spread until they reach a concentration in which they can no longer grow (TMP, Fig. 1C and movies S1 and S2; CPR, movie S3). As resistant mutants arise in the population, their descendants migrate into the next step of drug concentration and fan out (Fig. 1C, 88 hours). Adjacent mutant lineages exclude each other and compete for limited space, resulting in some lineages entirely blocking off growth of others (Fig. 1C). When the winning lineages reach a further increased level of drug concentration at which they too are unable to grow, secondary mutations arise and the process repeats. Ultimately, the bacteria reach and overspread the highest drug concentration, showing marked increases in drug resistance: Phenotyping of sampled mutants from the highest-concentration region showed a factor of 10^4 increase in MIC for TMP (Fig. 1B) and a factor of 10^5 increase in MIC for CPR (fig. S1). The adaption time (10 days in TMP, 12 days in CPR) is consistent with evolution in well-mixed environments (*4*), yet is slower than reported adaptation rates in microspatial environments, likely because of the additional time required to swim between concentration steps (*9*). It is possible that at different dimensions, the MEGA-plate will yield different evolutionary dynamics; a wider front would increase the effective population size and thus the mutational supply, whereas a longer run between steps would increase selection among adjacent lineages.

To test the importance of the size of intermediate steps in the evolution of high-level resistance, we set up a variant of the MEGA-plate in which bacteria go from no drug to a high level directly or through one middle region of variable magnitude (Fig. 2; TMP: high step 3000 × MIC, middle step 0, 3, 30, or 300 × MIC; CPR: high step 2000 × MIC, middle step 0, 2, 20, or 200 × MIC). Bacteria were unable to adapt directly from zero to the highest concentration of either drug. Diffusive smoothing of these large steps enabled the appearance of partially resistant mutants, but their lineages did not advance (Fig. 2A, left). The addition of an intermediate concentration step enabled adaptation, although this was impeded when this middle step was too high (Fig. 2B). Even across the permissive intermediate steps, evolution often proceeded through multiple mutations taking advantage of the local gradients formed by diffusion (TMP, movie S4; CPR, movie S5). Thus, by progressing through colonization of regions with moderately challenging selective pressures, intermediate-resistance mutants can expand to sufficient numbers to facilitate the rise of high-resistance mutants. Analogous to evolutionary

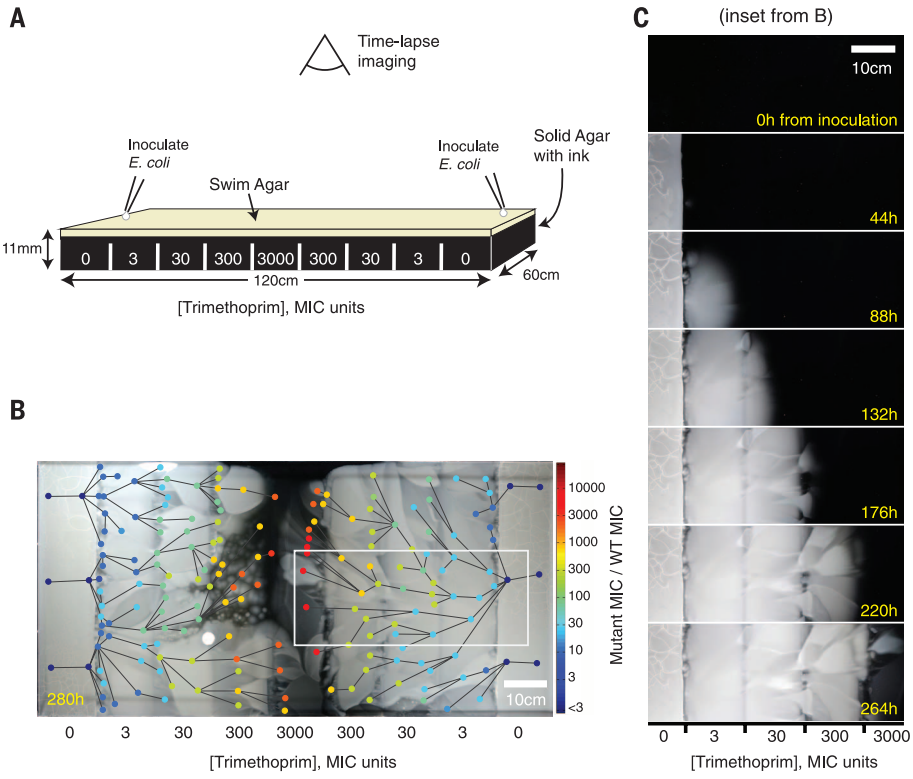

Fig. 1. An experimental device for studying microbial evolution in a spatially structured environment. (**A**) Setup of the four-step gradient of trimethoprim (TMP). Antibiotic is added in sections to make an exponential gradient rising inward. (**B**) The four-step TMP MEGA-plate after 12 days. *E. coli* appear as white on the black background. The 182 sampled points of clones are indicated by circles, colored by their measured MIC. Lines indicate video-imputed ancestry. (**C**) Time-lapse images of a section of the MEGA-plate. Repeated mutation and selection can be seen at each step. Images have been aligned and linearly contrast-enhanced but are otherwise unedited.

[1]Department of Systems Biology, Harvard Medical School, Boston, MA, USA. [2]Faculty of Biology, Technion–Israel Institute of Technology, Haifa, Israel. [3]Faculty of Computer Science, Technion–Israel Institute of Technology, Haifa, Israel. *Present address: Massachusetts Institute of Technology, Cambridge, MA, USA. †Present address: IST Austria, Klosterneuburg, Austria. ‡**Corresponding author. Email: rkishony@technion.ac.il**

rescue in temporal selective gradients (*18*–*20*), a gradual spatial gradient allows adaptation to previously inhospitable environments. However, unlike in a temporal gradient, a spatial gradient does not impose a minimal time for a mutant's appearance and spread; at any time, a mutant appearing on the stalled front can expand and evolve further, provided it is sufficiently resistant to colonize the next step. Thus, concordant with theoretical predictions (*21*, *22*), access to intermediate regions of moderate selection is critical for enabling a range of evolutionary paths to high-level resistance.

We next focused on the genotypic and phenotypic paths leading to high levels of resistance. We sequenced 21 isolates from the four-step TMP gradient experiment and 230 isolates from the multiple intermediate-step TMP experiment above. The samples separated into minimally and highly mutated (i.e., mutator phenotype) groups [>60 single-nucleotide polymorphisms (SNPs) and indels for high, <12 for low; Fig. 3A]. Similar separation was also seen when restricting the analysis to synonymous mutations to minimize differential effects of selection (fig. S2). All highly mutated isolates, but none of the others, had mutations in *dnaQ* (also called *mutD*), which was the only gene for which the presence of a mutation correlated perfectly with the mutator phenotype. This gene encodes DNA polymerase III, which is critical to proofreading (*23*, *24*). Isolates carrying mutated *dnaQ* alleles showed increased rates of mutations on rifampin disk diffusion assays (fig. S2) (*25*). These mutators appeared repeatedly in distinct locations on the plate and across experiments. On the basis of lineage reconstructions from the time-lapse video as well as genotypic relationships, the mutator phenotype emerged at least six times independently between the four-step and intermediate-step TMP experiments above [fig. S2; four different alleles of *dnaQ* were observed: $Val^{96} \rightarrow$ Glu (V96E), $Ile^{97} \rightarrow$ Asn (I97N), $Ile^{97} \rightarrow$ Ser (I97S), and $Ile^{97} \rightarrow$ Thr (I97T), where I97T appeared three independent times]. Although these mutator lineages accumulated mutations more rapidly, their rate of phenotypic adaption was similar to that of the less mutated isolates, reaching the highest level of resistance at roughly the same time (fig. S3 and movie S4). Indeed, the highly mutated lineages had a close to neutral ratio of nonsynonymous to synonymous substitutions (Fig. 3B). In contrast, the less mutated isolates showed a high bias toward coding mutations, indicating that most of these mutations were likely adaptive (Fig. 3B).

Focusing on the nonmutator isolates, we identified a wide spectrum of putatively adaptive mutations for TMP resistance. The most frequently mutated gene was the primary target of TMP, *folA* (*26*), which encodes dihydrofolate reductase (DHFR) (Fig. 3C), with more mutations appearing as resistance increased. We also observed several genes that were repeatedly mutated yet are not involved in the folate biosynthesis pathway, and thus are not primarily associated with TMP resistance. These included stress response genes, such as those of the *mar* and *sox* operons, known to be important in general antibiotic and toxin resistance (*27*), as well as genes involved in transcription and translation, which have been shown to affect TMP resistance (*28*). We also found that three genes not classically associated with TMP resistance were repeatedly mutated, often with a probable loss of function (frameshift or nonsense): a phosphate transporter (*pitA*), shikimate kinase I (*aroK*), and a negative regulator of the PhoQP system (*mgrB*). Knockout of these genes in the ancestral strain confirmed their resistance phenotypes (fig. S4).

Mutations that increased resistance often came with a cost of reduced growth, which was subsequently restored by additional compensatory mutations (*29*–*31*). Although some resistance-conferring mutations allowed colonization of regions of high drug concentration without affecting growth, many lineages capable of growing in these regions were deficient in yield, particularly during CPR resistance evolution (as measured by optical density: Fig. 4, A and B, for CPR; fig. S3 for TMP). These yield-deficient mutations were followed by compensatory mutations allowing growth to full density (Fig. 4, A and B, and movie S3; number of compensatory mutants observed in a single run: >50 for TMP, >500 for CPR). In the absence of a chemotaxis-inducing nutrient gradient, the compensatory mutants stayed localized behind the front, appearing in a characteristic pattern of localized spots spreading from single points (Fig. 4A and movie S3).

Focusing on evolution in CPR, we sampled and phenotyped compensatory mutants. We found that many of them had not only compensated for growth but had also increased in resistance, often beyond the resistance levels of the propagating front (Fig. 4C). Yet, as these mutants were engulfed by their parental lineage, they stayed constrained to the immediate vicinity in which they appeared and were unable to overtake the moving front. To test whether these compensatory mutants were capable of outcompeting the propagating front, we conducted an additional evolution experiment in

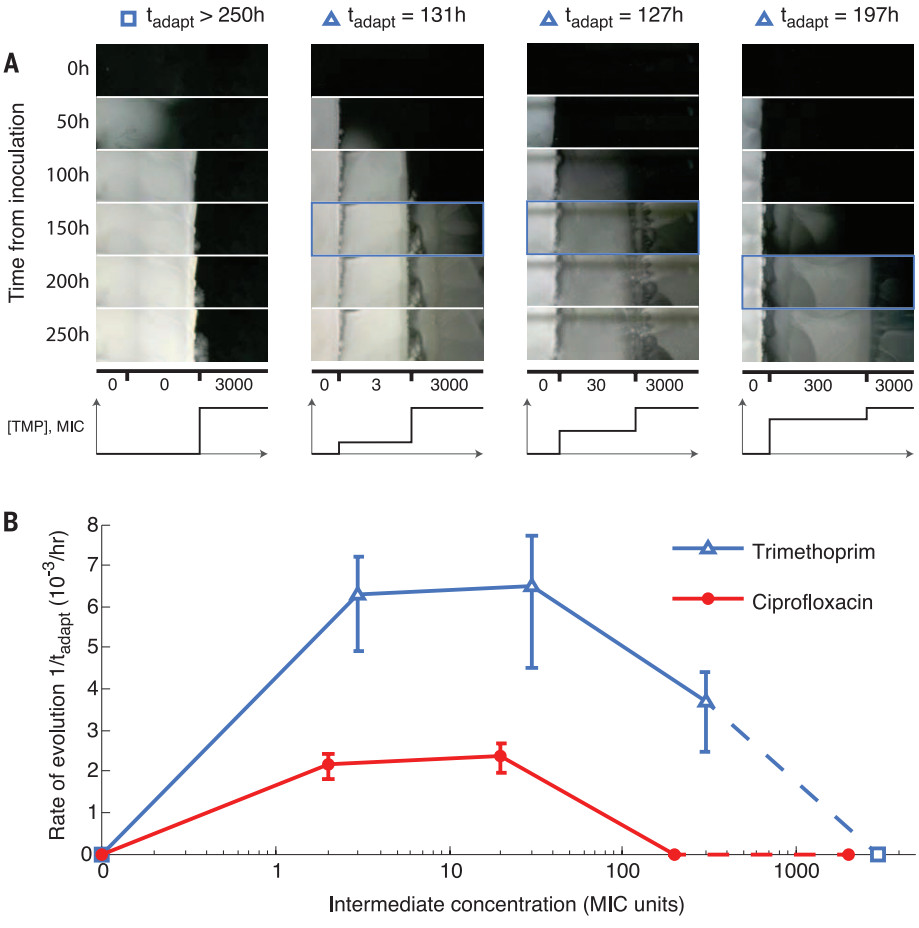

Fig. 2. Initial adaptation to low drug concentrations facilitates later adaptation to high concentrations. (**A**) Frames from a section of the TMP intermediate-step MEGA-plate over time (TMP, movie S4; CPR, movie S5). The first frame showing a mutant in the highest band is indicated by a blue box. (**B**) Rates of adaptation in the intermediate-step experiments across TMP and CPR, showing the necessity of intermediate adaptation for the evolution of high levels of resistance. Error bars show the appearance times of multiple lineages in the highest concentration. Because the intermediate step with no drug puts the highest and lowest concentrations adjacent, it serves as both the highest and lowest intermediate steps (dashed line).

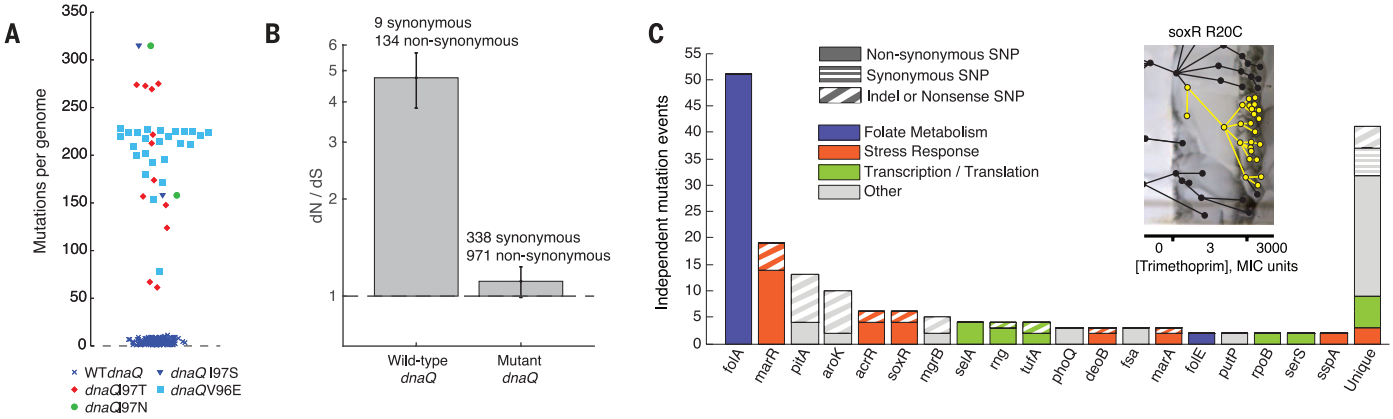

Fig. 3. Diverse genotypic strategies for adaptation to trimethoprim. (**A**) Numbers of observed mutations across individual isolates. Samples with a *dnaQ* mutation (solid symbols) consistently carried more mutations than those sampled with the wild-type *dnaQ* allele (crosses). Data points are horizontally jittered for clarity. (**B**) The normalized ratio of nonsynonymous to synonymous substitutions of isolates compared with the ancestor for samples with normal and highly mutated phenotypes. Error bars are the standard deviation of the Bayesian posterior estimate for the binomial parameter. (**C**) Numbers of distinct mutational events in genes that were mutated at least twice independently. Genes are colored by pathway per EcoCyc (*37*). Nonsynonymous, synonymous, and loss-of-function mutations (including indel and nonsense) are indicated. Genes that only had one mutation across all samples were combined into the "unique" column. Individual mutation events were inferred through ancestry (movies S1 and S4). Inset: The multistep MEGA-plate with samples containing the mutation *soxR* R20C (yellow) tracing mutational events from multiple samples and video.

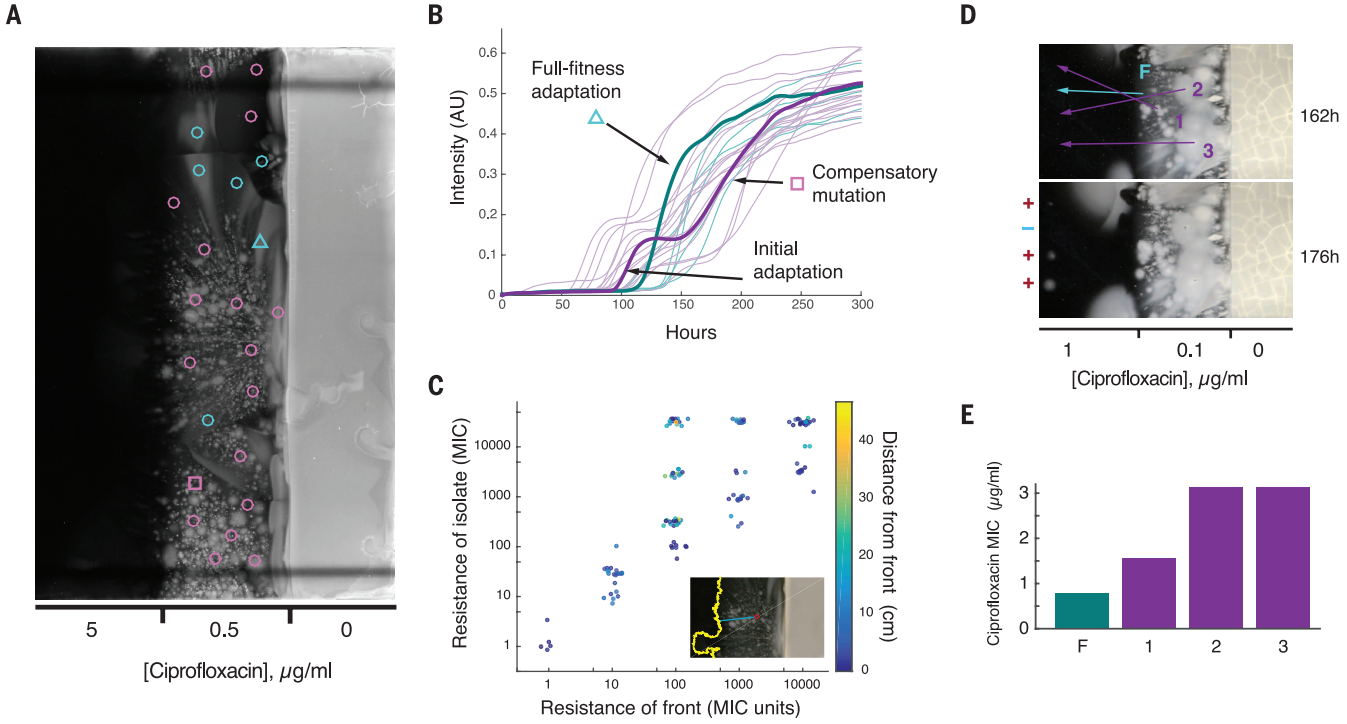

Fig. 4. Compensatory mutations can be spatially trapped. (**A**) Ciprofloxacin experiment still frame with locations of 24 isolates showing a full-fitness mutation (cyan) or yield-deficient mutation followed by a compensatory mutation (purple). (**B**) Optical density at the marked points in (A) over the course of the experiment. The two example traces (indicated by a square and triangle) correspond to the points marked by the same glyph in (A). (**C**) Mutants isolated behind the front can have markedly higher resistance than the front at the time it passed the same location. Resistance of the front was measured by the concentration at which front progression stopped; isolate MICs were measured in vitro. (**D**) The front (marked F) and three compensatory mutants (marked 1 to 3) were sampled at 162 hours, and immediately inoculated ahead of the front as indicated by the arrows. Growth of the moved mutants is evident for the three compensatory mutants, despite being inoculated at a CPR concentration much higher than where they emerged, but not for the front. (**E**) Measured CPR MICs of the mutants from (D).

which we sampled the trapped compensatory mutants and moved them forward, reinoculating them ahead of the still-moving front. These compensatory mutants were able to grow in a region where the front could not (Fig. 4D). Similarly, some trapped compensatory mutants were able to outcompete their parent when placed side-by-side on a fresh gradient plate (fig. S5). Hence, as compensatory mutations often occur behind the front, they are spatially restricted from contributing to the ultimate evolutionary course of the population. Indeed, in the rare cases

when these compensatory mutations appeared at the front and were not physically blocked, they accelerated the adaptive process (fig. S3 and movie S3, 00:53). Thus, the fitness of the population is not driven by the fittest mutants (*32*–*34*), but rather by those that are both sufficiently fit and arise sufficiently close to the advancing front.

The MEGA-plate is not intended to directly simulate natural or clinical settings, but it does capture unique aspects of evolution during range expansion. Evolution of high levels of resistance is enabled by intermediate regions of moderate selective pressure. Furthermore, as multiple lineages evolve in parallel, the propagating front can be led by lineages less fit than those trapped behind it. It will be interesting to explore how adaptation rates and mutational diversity depend on other spatiotemporal parameters, including population density, mutation rate, and the relative expansion speed and spatial dimensions. Owing to the relaxed evolutionary constraints in range expansion dynamics, the MEGA-plate is likely to reveal novel mutational pathways to high-level multiantibiotic resistance. Further, the MEGA-plate can be adapted to a range of organisms and challenges beyond antibiotics. Differences in evolutionary dynamics between evolution under different selection pressures appear visually, simplifying both hypothesis generation and testing. Owing to this flexibility, the MEGA-plate is a platform for exploring the interplay of spatial constraints and evolutionary pressures. The MEGA-plate provides a physical analog of the otherwise abstract Muller plots of population genetics (*35*, *36*) and of other elusive aspects of evolution, including diversification, compensatory mutations, and clonal interference. Its relative simplicity and ability to visually demonstrate evolution makes the MEGA-plate a useful tool for science education and outreach.

REFERENCES AND NOTES

1. D. M. Weinreich, N. F. Delaney, M. A. Depristo, D. L. Hartl, *Science* **312**, 111–114 (2006).
2. H. H. Lee, M. N. Molla, C. R. Cantor, J. J. Collins, *Nature* **467**, 82–85 (2010).
3. P. G. Lane, A. Hutter, S. G. Oliver, P. R. Butler, *Biotechnol. Prog.* **15**, 1115–1124 (1999).
4. E. Toprak *et al*., *Nat. Genet.* **44**, 101–105 (2012).
5. L. Imamovic, M. O. A. Sommer, *Sci. Transl. Med.* **5**, 204ra132 (2013).
6. V. Lázár *et al*., *Mol. Syst. Biol.* **9**, 700–700 (2013).
7. O. Fridman, A. Goldberg, I. Ronin, N. Shoresh, N. Q. Balaban, *Nature* **513**, 418–421 (2014).
8. M. Hegreness, N. Shoresh, D. Damian, D. Hartl, R. Kishony, *Proc. Natl. Acad. Sci. U.S.A.* **105**, 13977–13981 (2008).
9. Q. Zhang *et al*., *Science* **333**, 1764–1767 (2011).
10. T. M. Conrad, N. E. Lewis, B. O. Palsson, *Mol. Syst. Biol.* **7**, 509–509 (2011).
11. T. J. Kawecki *et al*., *Trends Ecol. Evol.* **27**, 547–560 (2012).
12. J. L. Martínez, *Proc. Biol. Sci.* **276**, 2521–2530 (2009).
13. O. Hallatschek, P. Hersen, S. Ramanathan, D. R. Nelson, *Proc. Natl. Acad. Sci. U.S.A.* **104**, 19926–19930 (2007).
14. P. Greulich, B. Waclaw, R. J. Allen, *Phys. Rev. Lett.* **109**, 088101 (2012).
15. R. Hermsen, J. B. Deris, T. Hwa, *Proc. Natl. Acad. Sci. U.S.A.* **109**, 10775–10780 (2012).
16. H. C. Berg, D. A. Brown, *Nature* **239**, 500–504 (1972).
17. J. B. Xavier, K. R. Foster, *Proc. Natl. Acad. Sci. U.S.A.* **104**, 876–881 (2007).
18. G. Bell, A. Gonzalez, *Science* **332**, 1327–1330 (2011).
19. A. Gonzalez, G. Bell, *Philos. Trans. R. Soc. London Ser. B* **368**, 20120079 (2013).
20. H. A. Lindsey, J. Gallie, S. Taylor, B. Kerr, *Nature* **494**, 463–467 (2013).
21. J. R. Bridle, T. H. Vines, *Trends Ecol. Evol.* **22**, 140–147 (2007).
22. J. Polechová, N. H. Barton, *Proc. Natl. Acad. Sci. U.S.A.* **112**, 6401–6406 (2015).
23. R. G. Fowler, G. E. Degnen, E. C. Cox, *Mol. Gen. Genet.* **133**, 179–191 (1974).
24. H. Echols, C. Lu, P. M. Burgers, *Proc. Natl. Acad. Sci. U.S.A.* **80**, 2189–2192 (1983).
25. J.-C. Galán *et al*., *J. Clin. Microbiol.* **42**, 4310–4312 (2004).
26. D. R. Smith, J. M. Calvo, *Mol. Gen. Genet.* **187**, 72–78 (1982).
27. R. G. Martin, K. W. Jair, R. E. Wolf Jr., J. L. Rosner, *J. Bacteriol.* **178**, 2216–2223 (1996).
28. T. Bollenbach, S. Quan, R. Chait, R. Kishony, *Cell* **139**, 707–718 (2009).
29. R. E. Lenski, *Int. Microbiol.* **1**, 265–270 (1998).
30. B. R. Levin, V. Perrot, N. Walker, *Genetics* **154**, 985–997 (2000).
31. A. Handel, R. R. Regoes, R. Antia, *PLOS Comput. Biol.* **2**, e137 (2006).
32. C. O. Wilke, J. L. Wang, C. Ofria, R. E. Lenski, C. Adami, *Nature* **412**, 331–333 (2001).
33. R. Sanjuán, J. M. Cuevas, V. Furió, E. C. Holmes, A. Moya, *PLOS Genet.* **3**, e93 (2007).
34. F. M. Codoñer, J.-A. Darós, R. V. Solé, S. F. Elena, *PLOS Pathog.* **2**, e136 (2006).
35. H. J. Muller, *Am. Nat.* **66**, 118–138 (1932).
36. J. E. Barrick, R. E. Lenski, *Nat. Rev. Genet.* **14**, 827–839 (2013).
37. I. M. Keseler *et al*., *Nucleic Acids Res.* **41**, D605–D612 (2013).

ACKNOWLEDGMENTS

Sequence data are available on NCBI SRA under accession number SRP077287. We thank X. R. Bao and A. C. Palmer for helpful discussions and the National BioResource Project (NIG, Japan) for providing the Keio collection. Supported by National Defense Science and Engineering Graduate fellowship 32 CFR 168a (E.D.K.), NIH grant R01-GM081617 (R.K.), and European Research Council FP7 ERC grant 281891 (R.K.).

SUPPLEMENTARY MATERIALS

www.sciencemag.org/content/353/6304/1147/suppl/DC1
Materials and Methods
Figs. S1 to S6
Tables S1 and S2
Movies S1 to S5
References (*38*–*43*)

6 May 2016; accepted 28 July 2016
10.1126/science.aag0822

INTERNET ACCESS

Digital discrimination: Political bias in Internet service provision across ethnic groups

Nils B. Weidmann,[1]* Suso Benitez-Baleato,[1,2] Philipp Hunziker,[3] Eduard Glatz,[4] Xenofontas Dimitropoulos[5,6]

The global expansion of the Internet is frequently associated with increased government transparency, political rights, and democracy. However, this assumption depends on marginalized groups getting access in the first place. Here we document a strong and persistent political bias in the allocation of Internet coverage across ethnic groups worldwide. Using estimates of Internet penetration obtained through network measurements, we show that politically excluded groups suffer from significantly lower Internet penetration rates compared with those in power, an effect that cannot be explained by economic or geographic factors. Our findings underline one of the central impediments to "liberation technology," which is that governments still play a key role in the allocation of the Internet and can, intentionally or not, sabotage its liberating effects.

In the wake of the Arab Spring, the Internet has often been portrayed as a "liberation technology" (*1*). Specifically, it has been argued that the Internet fosters transparency and accountability of nondemocratic governments worldwide and can help opposition movements organize for collective action (*2*). This expectation, however, is based on the assumption that political activists have sufficient access to the Internet in the first place.

The socioeconomic background of individuals affects their access to the Internet (*3*, *4*). Also, there is evidence of a global digital divide: Countries with democratic institutions and higher levels of development have higher Internet penetration rates (*5*). Still, we do not know how the provision of Internet services varies across societal groups in a country or how it is driven by politics. This information is key if we are to assess whether the Internet can indeed empower politically marginalized populations.

In most developing countries, governments are the major, if not the only, provider of telecommunication services (*6*). At the same time, in many of these countries, politics operates along ethnic lines, so that one or more groups hold

[1]Department of Politics and Public Administration, University of Konstanz, Universitätsstraße 10, 78457 Konstanz, Germany. [2]Department of Political Science, University of Santiago de Compostela, Campus Vida, 15705 Compostela, Spain. [3]International Conflict Research, ETH Zurich, Haldeneggsteig 4, 8092 Zurich, Switzerland. [4]Computer Engineering and Networks Laboratory, ETH Zurich, Gloriastraße 35, 8092 Zurich, Switzerland. [5]Foundation for Research and Technology Hellas, Nikolaou Plastira 100, 71110 Heraklion, Crete, Greece. [6]Department of Computer Science, University of Crete, Voutes Campus, 70013 Heraklion, Crete, Greece.
***Corresponding author. Email: nils.weidmann@uni-konstanz.de**